electronic reprint

STRUCTURAL BIOLOGY
COMMUNICATIONS

ISSN: 2053-230X
journals.iucr.org/f

Crystallization and X-ray diffraction analysis of SpaE, a basal pilus protein from the gut-adapted *Lactobacillus rhamnosus* GG

Arjun K. Mishra, Abhin Kumar Megta, Airi Palva, Ingemar von Ossowski and Vengadesan Krishnan

Acta Cryst. (2017). F**73**, 321–327

STRUCTURAL BIOLOGY COMMUNICATIONS

ISSN 2053-230X

Crystallization and X-ray diffraction analysis of SpaE, a basal pilus protein from the gut-adapted *Lactobacillus rhamnosus* GG

Arjun K. Mishra,[a]‡ Abhin Kumar Megta,[a,b]‡ Airi Palva,[c] Ingemar von Ossowski[c] and Vengadesan Krishnan[a]*

[a]Laboratory of Structural Biology, Regional Centre for Biotechnology, NCR Biotech Science Cluster, Faridabad 121 001, India, [b]School of Biotechnology, KIIT University, Odisha 751 024, India, and [c]Department of Veterinary Biosciences, University of Helsinki, Helsinki, Finland. *Correspondence e-mail: kvengadesan@rcb.res.in

Received 6 April 2017
Accepted 9 May 2017

Edited by R. L. Stanfield, The Scripps Research Institute, USA

‡ These authors contributed equally.

Keywords: adhesion; probiotics; basal pilin; host–microbe interaction; sortase-dependent pili; *Lactobacillus rhamnosus* GG; SpaE.

Supporting information: this article has supporting information at journals.iucr.org/f

SpaE is the predicted basal pilin subunit in the sortase-dependent SpaFED pilus from the gut-adapted and commensal *Lactobacillus rhamnosus* GG. Thus far, structural characterization of the cell-wall-anchoring basal pilins has remained difficult and has been limited to only a few examples from pathogenic genera and species. To gain a further structural understanding of the molecular mechanisms that are involved in the anchoring and assembly of sortase-dependent pili in less harmful bacteria, *L. rhamnosus* GG SpaE for crystallization was produced by recombinant expression in *Escherichia coli*. Although several attempts to crystallize the SpaE protein were unsuccessful, trigonal crystals that diffracted to a resolution of 3.1 Å were eventually produced using PEG 3350 as a precipitant and high protein concentrations. Further optimization with a combination of additives led to the generation of SpaE crystals in an orthorhombic form that diffracted to a higher resolution of 1.5 Å. To expedite structure determination by SAD phasing, selenium-substituted (orthorhombic) SpaE crystals were grown and X-ray diffraction data were collected to 1.8 Å resolution.

1. Introduction

Among the Gram-positive bacteria, a number of genera and species are able to display sortase-dependent pili on their cell surfaces (Proft & Baker, 2009; Telford *et al.*, 2006; Ton-That & Schneewind, 2004). These lengthy and proteinaceous appendages exhibit a macromolecular architecture that typically consists of three types of protein subunits called pilins. Here, as first demonstrated in *Corynebacterium diphtheriae*, a repeating number of major pilins form the pilus backbone, with minor ancillary pilins located at the tip for adhesion and at the base for cell-wall anchoring (Mandlik, Swierczynski *et al.*, 2008; Ton-That & Schneewind, 2004). Characteristically, the various pilins are covalently linked together by a pilin-specific C-type sortase, whereas a housekeeping A-type sortase catalyzes the formation of a covalent bond between the basal pilin and the cell wall to anchor the assembled pilus. Although the basal pilins are mainly located at the pilus base and facilitate pilus cell-wall anchoring and termination, they are also occasionally observed within the pilus backbone and sometimes participate in adhesion (Krishnan *et al.*, 2007; Mandlik, Das *et al.*, 2008; Mandlik, Swierczynski *et al.*, 2008).

While sortase-dependent piliation has been well founded in pathogens (Mandlik, Swierczynski *et al.*, 2008; Proft & Baker,

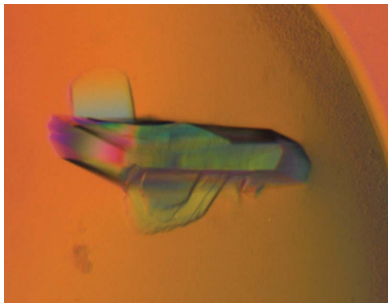

Table 1
Macromolecule-production information.

Source organism	*L. rhamnosus* GG (ATCC 53103)
DNA source	*L. rhamnosus* GG (ATCC 53103)
Forward primer†	5′-CCACATTGGGTTCAGAATTCTGATCAAACTG
Reverse primer‡	5′-TGCGCCAATCGGACTCGAGCGGCAAATAAC
Cloning vector	pET-28b(+) (Novagen)
Expression vector	pET-28b(+) (Novagen)
Expression host	*E. coli* BL21 (DE3) pLysS
Complete amino-acid sequence of the construct produced§	MGRDPNSDQTAEIVIHKRIYRDIRQPEDVWYEND-GHRIDPNNPDKDGYKLLSKTSGLNGANFEVYD-ASSLLKPNMTPEAIRALVDRYQNMTRKQALKF-ARANLKLAGQGNKGIGLMNTKNDPTLGEDGIS-RITVSVDQQAPTKAYLMIEVAPDPSTELNVDL-ERKSSPMLVVFPVTDPISGNPLQTIHLYPKNV-GYVRDPYFFKFGVHPDGTSKRLAGAIFAIYRI-ENGKKLYLDMSPVTDLRNKWVSTTDPLHDDRV-NKFVSDQDGLVNTGERFLPAGEYFFEELQGVP-GYEVDAKSRAIKIEIPDSWEDEDGNRRFVLID-GQPMQENFGGVVTPEMISSGYPRVYNYADKQA-STTGDQTAGPSTTQLGNHGQDTNGTGTRTPKR-QSGYLPLEHHHHHH

† The EcoRI site is underlined. ‡ The XhoI site is underlined. § The cloning artifacts are underlined.

2009; Telford *et al.*, 2006), it has only recently been recognized in the less harmful commensal bacteria (Kankainen *et al.*, 2009; Lebeer *et al.*, 2009; Turroni *et al.*, 2013; Yu *et al.*, 2015; Krishnan *et al.*, 2016). Among the latter is *Lactobacillus rhamnosus* GG, a gut-adapted strain that has been advocated to have various health benefits (Gorbach, 2000) and the genome of which contains operons (*spaCBA* and *spaFED*) that encode two different types of sortase-dependent pili (Kankainen *et al.*, 2009). One of these pilus types is called SpaCBA and is made up of the tip SpaC, basal SpaB and backbone SpaA pilins (Reunanen *et al.*, 2012), whereas the other is called SpaFED and is comprised of the tip SpaF, basal SpaE and backbone SpaD pilins (Rintahaka *et al.*, 2014). Owing to the constitutive expression of the fimbrial *spaCBA* operon in *L. rhamnosus* GG, the SpaCBA pilus is generally better studied than the SpaFED pilus, the operon for which shows no native expression under laboratory conditions (Reunanen *et al.*, 2012). Nonetheless, the *spaFED* genes were recently cloned in *Lactococcus lactis* to produce a recombinant form of the SpaFED pilus (Figs. 1*a* and 1*b*), which underwent functional and structural characterization (Rintahaka *et al.*, 2014). In terms of function, both pilus types can bind to intestinal mucus, an ability attributed to the SpaC, SpaB and SpaF ancillary pilins (Kankainen *et al.*, 2009; von Ossowski *et al.*, 2010). Moreover, they can also adhere to extracellular matrix proteins (*i.e.* collagen *via* SpaC and SpaF, and fibronectin *via* SpaF; Rintahaka *et al.*, 2014; Tripathi *et al.*, 2013) and gut epithelial cells (Ardita *et al.*, 2014; Lebeer *et al.*, 2012). Whereas only the SpaCBA pilus is correlated with biofilm development (Lebeer *et al.*, 2012; Yu *et al.*, 2015), both of these pilus types are involved in eliciting some form of host immune-cell response (Ardita *et al.*, 2014; Ganguli *et al.*, 2015; Lebeer *et al.*, 2012; Rintahaka *et al.*, 2014; Tytgat *et al.*, 2016; Vargas García *et al.*, 2015; von Ossowski *et al.*, 2013). However, as only the SpaCBA pilus is produced natively in *L. rhamnosus* GG cells, its functionality can be linked to helping to extend the transient colonization of the gut by this strain. On the other hand, despite the fimbrial *spaFED* operon being widespread among three *Lactobacillus* species (other strains of *L. rhamnosus*, *L. casei* and *L. paracasei*; Kant *et al.*, 2014), how its gene expression is activated remains under conjecture and unknown, although it might well be triggered by the gut *in situ* or by some other environmental factor. For instance, the Tad (tight adherence) pilus is an essential host-colonization factor and its expression in *Bifidobacterium breve* UCC2003 appears to be gut-induced and thus only observed *in vivo* (O'Connell Motherway *et al.*, 2011)

The use of X-ray crystallography has been instrumental in obtaining high-resolution structures of various Gram-positive pilin subunits, and accordingly this has helped in understanding the processes behind the anchoring, assembly and function of sortase-dependent pili (Kang & Baker, 2012; Krishnan, 2015; Vengadesan & Narayana, 2011). However, obtaining diffraction-quality crystals of the ancillary basal pilins remains a particular challenge, as they are relatively less stable than the major pilins. Consequently, only a limited number of basal pilin structures have become available, *i.e.* those of GBS52 from *Streptococcus agalactiae* (Krishnan *et al.*, 2007), FctB from *S. pyogenes* (Linke *et al.*, 2010) and RrgC from *S. pneumoniae* (Shaik *et al.*, 2014). In order to reveal additional mechanistic insight at the molecular level, we have

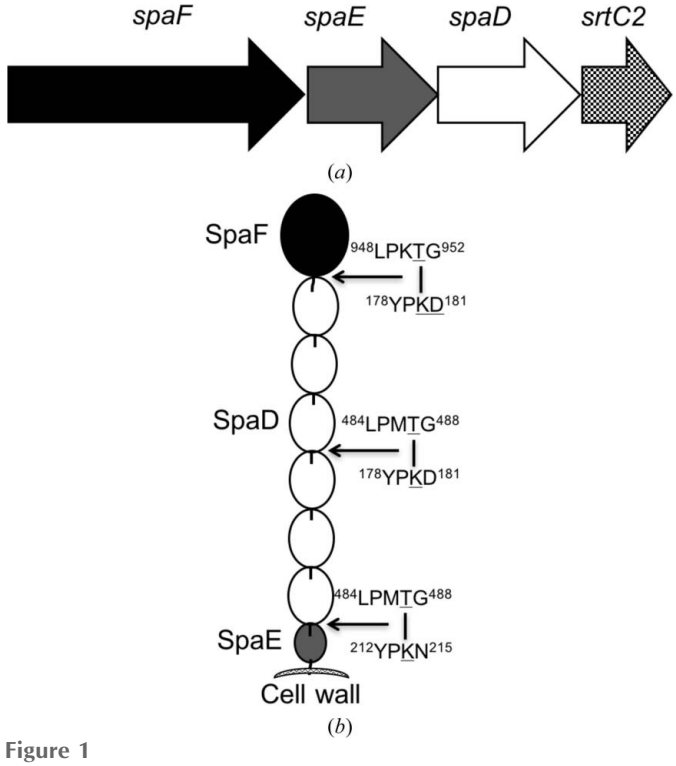

Figure 1
Schematic representations of the gene organization of the *L. rhamnosus* GG *spaFED* operon (*a*) and the assembled SpaFED pilus (*b*). Operon-associated genes (*spaF*, *spaE* and *spaD*) and their corresponding pilin-protein products (SpaF, SpaE and SpaD) are identified by matching greyscales. The possible sortase-mediated covalent cross-linking among the pilus subunits between the threonine from the C-terminal LP*X*TG sorting motif and the lysine from the YPKN pilin motif (Supplementary Fig. S1) is marked.

Table 2
Crystallization.

	Trigonal form (native)	Orthorhombic form (native)	Orthorhombic form (SeMet derivative)
Method	Hanging-drop vapour diffusion	Hanging-drop vapour diffusion	Hanging-drop vapour diffusion
Plate type	VDX plate (Hampton Research)	VDX plate (Hampton Research)	VDX plate (Hampton Research)
Temperature (K)	295	295	295
Protein concentration (mg ml^{-1})	100	100	100
Buffer composition of protein solution	50 m*M* Tris–HCl pH 8.0, 150 m*M* NaCl, 0.1 *M* bis-tris propane pH 8.5, 0.3 *M* sodium formate, 22% PEG 3350	50 m*M* Tris–HCl pH 8.0, 150 m*M* NaCl, 0.1 *M* bis-tris propane pH 8.5, 0.25 *M* sodium formate, 25% PEG 3350, 0.2 *M* sodium iodide, 0.02 *M* L-proline	50 m*M* Tris–HCl pH 8.0, 150 m*M* NaCl, 0.1 *M* bis-tris propane pH 8.5, 0.3 *M* sodium formate, 30% PEG 3350, 1 *M* sodium iodide, 0.1 *M* L-proline
Volume and ratio of drop	2 µl, 1:1	2 µl, 1:1	2 µl, 1:1
Volume of reservoir (ml)	1	1	1

undertaken a structural investigation of the pilin subunits in *L. rhamnosus* GG (Chaurasia *et al.*, 2015, 2016; Kant *et al.*, 2016). Here, we report the crystallization and X-ray diffraction analysis of SpaE, which represents the first basal subunit from a commensal-derived pilus.

2. Materials and methods

2.1. Macromolecule production

A plasmid construct containing residues 30–414 of the *L. rhamnosus* GG (ATCC 53103) *spaE* gene was generated in *Escherichia coli* BL21 (DE3) pLysS strain (Table 1; von Ossowski *et al.*, 2010). This plasmid construct does not have the N-terminal secretion and C-terminal LP*X*TG sorting signals, but contains a hexahistidine tag at the C-terminus. For the production of SpaE, the *E. coli* cells were grown at 303 K in Luria–Bertani (LB) medium containing 50 µg ml^{-1} kanamycin until an OD_{600} of 0.6 was reached, at which point protein expression was induced by adding isopropyl β-D-1-thiogalactopyranoside (IPTG) to a final concentration of 1 m*M*. After overnight incubation at 303 K, the cells were centrifugally pelleted and resuspended in lysis buffer (40 m*M* sodium phosphate buffer pH 8, 400 m*M* NaCl, 10 m*M* imidazole) supplemented with EDTA-free protease inhibitors (Roche). The cell suspension was disrupted by sonication and the lysate was centrifuged at 48 400*g* for 40 min at 277 K to remove cellular debris. The cell-free supernatant was loaded onto an Ni^{2+}-charged 5 ml HiTrap Chelating HP column (GE Healthcare) pre-equilibrated with lysis buffer, which was then washed with lysis buffer containing 20 m*M* imidazole. Recombinant SpaE was removed from the column using a linear gradient of elution buffer (40 m*M* sodium phosphate pH 8, 400 m*M* NaCl, 400 m*M* imidazole) and its purity was judged by running the eluted fractions on a 12% SDS–polyacrylamide gel. SpaE-containing fractions were pooled, dialyzed overnight against 50 m*M* Tris–HCl pH 8, 150 m*M* NaCl at 277 K and subsequently concentrated using an Amicon ultrafiltration centrifugal device equipped with a 10 kDa cutoff membrane. Concentrated SpaE protein was further purified by size-exclusion chromatography using a Sephacryl 200 26/60 gel-filtration column (GE Healthcare) equilibrated with 50 m*M* Tris–HCl pH 8, 150 m*M* NaCl. For the production of a selenomethionine (SeMet) derivative of SpaE, the plasmid was transformed into the auxotrophic *E. coli* strain B834 and the cells were subsequently grown in SeMet Medium Base plus Nutrient Mix (Molecular Dimensions) and 50 mg l^{-1} L-SeMet. Protein expression and purification were performed as described above.

2.2. Circular dichroism

Prior to crystallization, circular-dichroism (CD) analysis of the SpaE protein at a final concentration of 0.2 mg ml^{-1} in 25 m*M* phosphate buffer pH 8 in a quartz cuvette (0.1 cm path length) was carried out using a Jasco J-815 CD spectrophotometer. CD spectra were recorded from 190 to 260 nm at 295 K using a 1.0 nm band width, with a data interval of 0.1 nm and a 1 s signal averaging time. The spectrum was plotted in units of mean molar residue ellipticity following the subtraction of buffer scans. A CD spectra analyser (a Jasco J-810 spectropolarimeter) was used to show the presence of secondary-structural elements.

2.3. Crystallization

Initial screening was performed at 295 K using the sitting-drop vapour-diffusion technique with an automated liquid-handing robotic system (Mosquito, TTP Labtech) and various commercially available kits. One of the conditions yielded small-sized crystals within two weeks when highly concentrated protein (100 mg ml^{-1}) was used. This condition was further optimized using the hanging-drop vapour-diffusion method to produce rod-shaped trigonal crystals (Table 2). To improve the diffraction quality of these crystals, additional screening was performed using various additives (Hampton Research). Further optimization was carried out with different combinations of the most promising additives to produce small-sized crystals. Following this, it was found that the combined use of sodium iodide and L-proline as additives greatly improved the diffraction quality, although the crystal form changed from trigonal to orthorhombic (Table 2). Protein crystals of SeMet-derivatized SpaE were obtained using the same crystallization conditions, in which orthorhombic crystals were grown and were then further optimized (Table 2).

2.4. Peptide mass fingerprinting analysis

To confirm the identity of the crystallized protein, peptide mass fingerprinting (PMF) analysis was carried out with an

Table 3
Data collection and processing.

Values in parentheses are for the outer shell.

	Trigonal form (native)	Orthorhombic form (native)	Orthorhombic form (SeMet derivative)
Diffraction source	BM14, ESRF	PX-BL-21, RRCAT	BM14, ESRF
Wavelength (Å)	0.97887	0.97947	0.97868
Temperature (K)	100	100	100
Detector	MAR CCD 225	MAR CCD 225	MAR CCD 225
Crystal-to-detector distance (mm)	303	160	168
Rotation range per image (°)	0.5	0.5	0.25
Total rotation range (°)	91	180	180
Exposure time per image (s)	8	15	3
Space group	$P3_121$ or $P3_221$	$P2_12_12_1$	$P2_12_12_1$
a, b, c (Å)	130.07, 130.07, 59.35	41.79, 64.21, 131.42	41.78, 63.94, 131.13
α, β, γ (°)	90, 90, 120	90, 90, 90	90, 90, 90
Mosaicity (°)	0.22	0.34	0.36
Resolution range (Å)	52.5–3.15 (3.32–3.15)	131.4–1.5 (1.58–1.50)	43.7–1.8 (1.90–1.80)
Total No. of reflections	57471	375460	237737
No. of unique reflections	10257	56764	33112
Completeness (%)	99.9 (100.0)	98.6 (90.7)	99.6 (97.6)
Multiplicity	5.6 (5.7)	6.6 (4.2)	7.2 (7.1)
$\langle I/\sigma(I)\rangle$	19.5 (2.6)	18.3 (3.1)	19.8 (4.0)
R_{meas}	0.08 (0.75)	0.06 (0.47)	0.08 (0.55)
Overall B factor from Wilson plot (Å^2)	35.1	17.9	33.3
ΔAnom correlation between half sets	—	—	0.72 (0.09)
Mid-Slope of Anom. Normal Probability	—	—	1.57

AB SCIEX MALDI-TOF 5800 mass-spectrometer system on a single protein band obtained by SDS–PAGE. Excised gel slices were subjected to repeated cycles of dehydration and rehydration, first with a 2:1 mixture of acetonitrile and 50 m*M* ammonium bicarbonate (ABC) for 5 min and subsequently with 25 m*M* ABC for 2 min. They were then trypsinized overnight at 37°C (20 mg ml^{-1} trypsin in 25 m*M* ABC) for mass-spectrometric analysis.

2.5. Data collection and processing

Initial X-ray diffraction analysis of the crystals was performed at our home source. High-resolution data were collected using a synchrotron source on beamlines BM14 at the ESRF, Grenoble, France and PX-BL-21 at RRCAT, Indore, India. During data collection, 2.1 *M* sodium formate and 1 *M* magnesium acetate tetrahydrate were used as cryo-protectants for the trigonal and orthorhombic crystal forms, respectively. An SeMet-derivatized SpaE crystal was used for single-wavelength anomalous dispersion (SAD) data collection at the peak wavelength on the BM14 beamline. The data were indexed and integrated with *XDS* (Kabsch, 2010), while further scaling was performed with *AIMLESS* from the *CCP*4 suite (Winn *et al.*, 2011) (Table 3).

3. Results and discussion

L. rhamnosus GG SpaE pilin subunit was produced recombinantly in *E. coli* cells as a soluble C-terminally hexahistidine-tagged protein (Table 1), and was subsequently purified using affinity and gel-filtration chromatography. The recombinant SpaE protein migrated on an SDS–polyacrylamide gel with a molecular weight of ∼45 kDa (Fig. 2*a*), which was in good agreement with the calculated molecular weight based on the cloned construct (44 776 Da). Estimation of the molecular weight based on the elution volume of standard proteins using size-exclusion chromatography suggested that the purified recombinant SpaE is homogeneous and monomeric in solution (Fig. 2*b*). CD spectral analysis of the purified SpaE protein showed the characteristic features of regular secondary structures with β-sheet as the major content, *i.e.* 60.7% β-sheet, 3.7% α-helices, 4.5% β-turns and 31% random coils (Fig. 3).

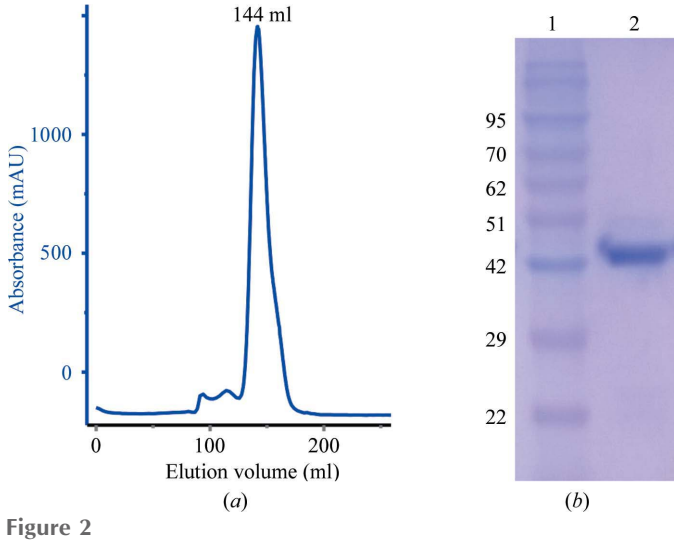

Figure 2
Purification and SDS–PAGE analysis of SpaE. (*a*) The two-step purification of recombinant SpaE protein involved nickel-affinity and gel-filtration chromatography. SpaE protein eluting at a volume of 140 ml corresponds to its monomeric form during final purification with a Sephacryl 200 26/60 size-exclusion column. (*b*) SDS–PAGE analysis of SpaE after the final purification step. Molecular-weight markers (lane 1; labelled in kDa) and purified ∼45 kDa SpaE protein (lane 2) are shown.

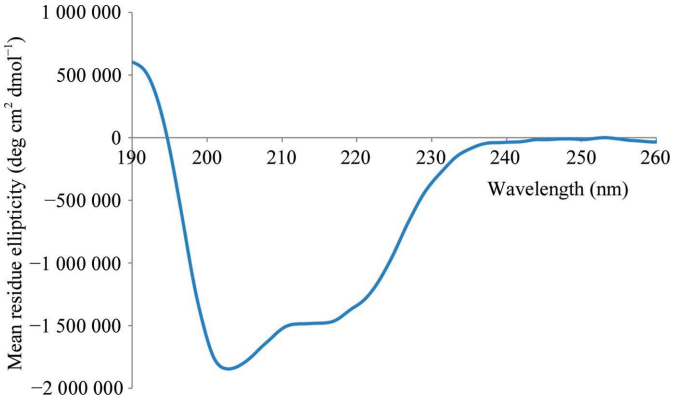

Figure 3
The far-UV circular-dichroism spectrum of SpaE.

In our preliminary crystallization screening trials, we used the same range of protein concentrations (*i.e.* 20–50 mg ml^{-1}) as we had used previously to obtain crystals of the *L. rhamnosus* GG SpaD and SpaA backbone pilins (Chaurasia *et al.*, 2015; Singh *et al.*, 2013). Presumably, the rather high solubility of SpaE caused the drops to remain mostly clear, although in about 5% of the drops some precipitation was observed. To remedy this, the SpaE protein samples were concentrated to progressively higher concentrations (*i.e.* 60, 70, 80, 90 and 100 mg ml^{-1}) and then used to screen for crystallization conditions. Ultimately, a 100 mg ml^{-1} concentration of SpaE protein was chosen, as within two weeks one of the screening conditions had yielded small-sized crystals. Optimization of this condition produced rod-shaped trigonal crystals (Fig. 4*a* and Table 2) that diffracted to a resolution of 3.1 Å (Fig. 5*a*)

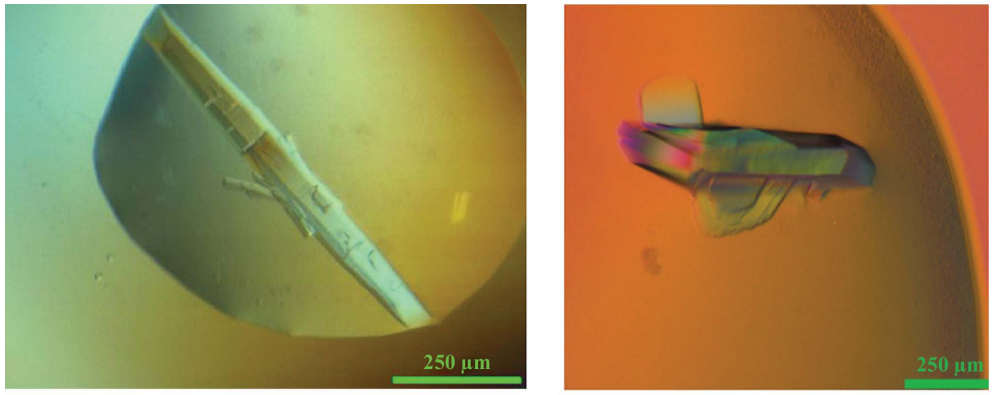

(*a*) (*b*)

Figure 4
SpaE crystallized by the vapour-diffusion method. (*a*) Trigonal crystals grown in a solution consisting of 0.3 *M* sodium formate, 0.1 *M* bis-tris propane pH 8.5, 22% PEG 3350. (*b*) Orthorhombic crystals grown in the same solution as above but with the additives 0.2 *M* sodium iodide and 0.02 *M* L-proline.

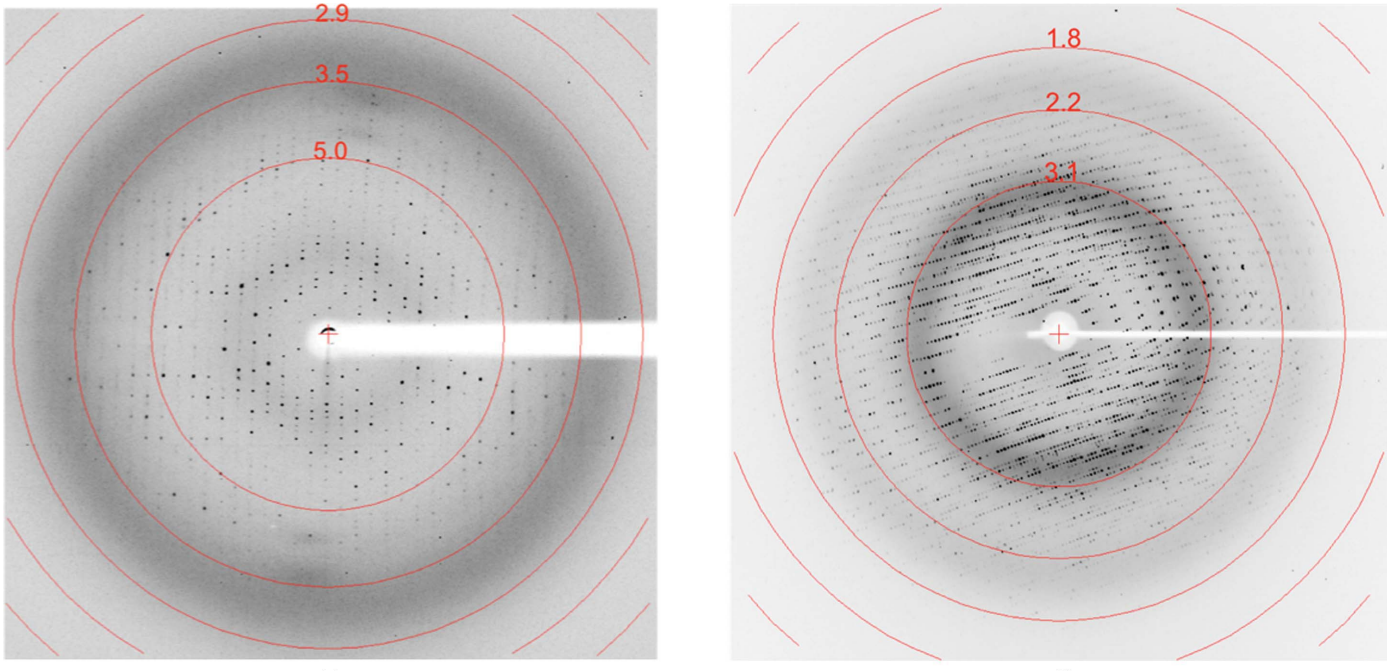

(*a*) (*b*)

Figure 5
X-ray diffraction patterns of SpaE crystals. (*a*) Diffraction pattern collected from a trigonal crystal on the BM14 beamline at the ESRF. (*b*) Diffraction pattern collected from an orthorhombic crystal on the PX-BL-21 beamline at RRCAT. Resolution arcs are indicated in Å (red circles).

on beamline BM14. After additional optimization with various additives, it was found that the combined use of sodium iodide and L-proline as additives improved the diffraction quality to 1.5 Å (Fig. 5*b*), although the crystal form changed from trigonal to orthorhombic (Fig. 4*b*). High-resolution data were collected from the orthorhombic crystal form on beamline PX-BL-21 (Table 3). To identify the crystallized protein as SpaE, the crystal sample was resolved by SDS–PAGE, with the corresponding protein band then subjected to in-gel trypsin digestion followed by PMF analysis (see Supplementary Fig. S1).

Matthews coefficient (V_M) analysis of both the trigonal (V_M = 3.22 Å^3 Da^{-1}, solvent content 61%) and orthorhombic (V_M = 1.96 Å^3 Da^{-1}, solvent content 38%) crystal forms indicated the presence of one molecule in the asymmetric unit. However, our attempts to solve the structure using molecular replacement and iodide-SAD phasing were unsuccessful owing to limited sequence identity to known pilin structures (see Supplementary Fig. S2) and the existence of a weak anomalous signal, respectively. Instead, SeMet-derivatized SpaE crystals were subsequently produced in the orthorhombic form (Table 2) and SAD data were collected at the peak wavelength (Table 3). Attempts are under way to solve the crystal structure by the use of selenium-SAD phasing. As the presence of a strong anomalous signal was observed in the data that were collected from the SeMet-derivatized SpaE crystal during scaling (ΔAnom correlation between half sets and Mid-Slope of Anom. Normal Probability in Table 3), this is likely to allow structure determination.

Acknowledgements

We acknowledge the support provided by the central instrumentation facility at RCB for mass-spectrometric and CD analysis and for home-source X-ray diffraction. We acknowledge the PX-BL-21 beamline (BARC) at Indus-2, RRCAT, Indore for high-resolution data collection and thank the beamline scientist Dr R. Makde for his support during data collection. We thank the EMBL staff Dr Hassan Belrhali and Dr Babu A. Manjasetty for providing support on the beamline and EMBL-DBT for providing access to the BM14 beamline at the ESRF. Operating costs and salaries at the University of Helsinki for the cloning of recombinant SpaE were funded by research grants from the Academy of Finland (Nos. 118165, 118602, 141140 and 277362).

Funding information

Funding for this research was provided by: Department of Biotechnology, Ministry of Science and Technology (award No. BT/PR5891/BRB/10/1098/2012).

References

Ardita, C. S., Mercante, J. W., Kwon, Y. M., Luo, L., Crawford, M. E., Powell, D. N., Jones, R. M. & Neish, A. S. (2014). *Appl. Environ. Microbiol.* **80**, 5068–5077.
Chaurasia, P., Pratap, S., von Ossowski, I., Palva, A. & Krishnan, V. (2016). *Sci. Rep.* **6**, 28664.
Chaurasia, P., von Ossowski, I., Palva, A. & Krishnan, V. (2015). *Acta Cryst.* F**71**, 103–106.
Ganguli, K., Collado, M. C., Rautava, J., Lu, L., Satokari, R., von Ossowski, I., Reunanen, J., de Vos, W. M., Palva, A., Isolauri, E., Salminen, S., Walker, W. A. & Rautava, S. (2015). *Pediatr. Res.* **77**, 528–535.
Gorbach, S. L. (2000). *Am. J. Gastroenterol.* **95**, S2–S4.
Kabsch, W. (2010). *Acta Cryst.* D**66**, 125–132.
Kang, H. J. & Baker, E. N. (2012). *Curr. Opin. Struct. Biol.* **22**, 200–207.
Kankainen, M. *et al.* (2009). *Proc. Natl Acad. Sci. USA*, **106**, 17193–17198.
Kant, R., Rintahaka, J., Yu, X., Sigvart-Mattila, P., Paulin, L., Mecklin, J. P., Saarela, M., Palva, A. & von Ossowski, I. (2014). *PLoS One*, **9**, e102762.
Kant, A., von Ossowski, I., Palva, A. & Krishnan, V. (2016). *Protein Pept. Lett.* **23**, 365–371.
Krishnan, V. (2015). *IUBMB Life*, **67**, 533–543.
Krishnan, V., Chaurasia, P. & Kant, A. (2016). *Probiotics and Prebiotics in Human Nutrition and Health*, edited by V. Rao & L. G. Rao, pp. 115–133. Rijeka: InTech.
Krishnan, V., Gaspar, A. H., Ye, N., Mandlik, A., Ton-That, H. & Narayana, S. V. L. (2007). *Structure*, **15**, 893–903.
Lebeer, S., Claes, I., Tytgat, H. L., Verhoeven, T. L., Marien, E., von Ossowski, I., Reunanen, J., Palva, A., de Vos, W. M., De Keersmaecker, S. C. J. & Vanderleyden, J. (2012). *Appl. Environ. Microbiol.* **78**, 185–193.
Lebeer, S., Verhoeven, T. L., Francius, G., Schoofs, G., Lambrichts, I., Dufrêne, Y., Vanderleyden, J. & De Keersmaecker, S. C. (2009). *Appl. Environ. Microbiol.* **75**, 3554–3563.
Linke, C., Young, P. G., Kang, H. J., Bunker, R. D., Middleditch, M. J., Caradoc-Davies, T. T., Proft, T. & Baker, E. N. (2010). *J. Biol. Chem.* **285**, 20381–20389.
Mandlik, A., Das, A. & Ton-That, H. (2008). *Proc. Natl Acad. Sci. USA*, **105**, 14147–14152.
Mandlik, A., Swierczynski, A., Das, A. & Ton-That, H. (2008). *Trends Microbiol.* **16**, 33–40.
O'Connell Motherway, M. *et al.* (2011). *Proc. Natl Acad. Sci. USA*, **108**, 11217–11222.
Ossowski, I. von, Pietilä, T. E., Rintahaka, J., Nummenmaa, E., Mäkinen, V. M., Reunanen, J., Satokari, R., de Vos, W. M., Palva, I. & Palva, A. (2013). *PLoS One*, **8**, e64416.
Ossowski, I. von, Reunanen, J., Satokari, R., Vesterlund, S., Kankainen, M., Huhtinen, H., Tynkkynen, S., Salminen, S., de Vos, W. M. & Palva, A. (2010). *Appl. Environ. Microbiol.* **76**, 2049–2057.
Proft, T. & Baker, E. N. (2009). *Cell. Mol. Life Sci.* **66**, 613–635.
Reunanen, J., von Ossowski, I., Hendrickx, A. P., Palva, A. & de Vos, W. M. (2012). *Appl. Environ. Microbiol.* **78**, 2337–2344.
Rintahaka, J., Yu, X., Kant, R., Palva, A. & von Ossowski, I. (2014). *PLoS One*, **9**, e113922.
Shaik, M. M., Maccagni, A., Tourcier, G., Di Guilmi, A. M. & Dessen, A. (2014). *J. Biol. Chem.* **289**, 16988–16997.
Singh, D., von Ossowski, I., Palva, A. & Krishnan, V. (2013). *Acta Cryst.* F**69**, 1182–1185.
Telford, J. L., Barocchi, M. A., Margarit, I., Rappuoli, R. & Grandi, G. (2006). *Nature Rev. Microbiol.* **4**, 509–519.
Ton-That, H. & Schneewind, O. (2004). *Trends Microbiol.* **12**, 228–234.
Tripathi, P., Beaussart, A., Alsteens, D., Dupres, V., Claes, I., von Ossowski, I., de Vos, W. M., Palva, A., Lebeer, S., Vanderleyden, J. & Dufrêne, Y. F. (2013). *ACS Nano*, **7**, 3685–3697.
Turroni, F. *et al.* (2013). *Proc. Natl Acad. Sci. USA*, **110**, 11151–11156.
Tytgat, H. L., van Teijlingen, N. H., Sullan, R. M., Douillard, F. P., Rasinkangas, P., Messing, M., Reunanen, J., Satokari, R., Vanderleyden, J., Dufrêne, Y. F., Geijtenbeek, T. B., de Vos, W. M. & Lebeer, S. (2016). *PLoS One*, **11**, e0151824.
Vargas García, C. E., Petrova, M., Claes, I. J., De Boeck, I.,

Verhoeven, T. L., Dilissen, E., von Ossowski, I., Palva, A., Bullens, D. M., Vanderleyden, J. & Lebeer, S. (2015). *Appl. Environ. Microbiol.* **81**, 2050–2062.
Vengadesan, K. & Narayana, S. V. L. (2011). *Protein Sci.* **20**, 759–772.
Winn, M. D. *et al.* (2011). *Acta Cryst.* D**67**, 235–242.
Yu, X., Jaatinen, A., Rintahaka, J., Hynönen, U., Lyytinen, O., Kant, R., Åvall-Jääskeläinen, S., von Ossowski, I. & Palva, A. (2015). *PLoS One*, **10**, e0145718.